VALUE-ADDED SIMULATION OF HYBRID SYSTEMS

Ian A. Hiskens*

Department of Electrical and Computer Engineering
University of Wisconsin-Madison

Email: `hiskens@engr.wisc.edu`

Abstract— Analytical investigations of real-world, hybrid dynamical systems are technically challenging. Consequently, simulation plays a vital role in their analysis. Simulation typically addresses forward problems though, offering limited insights into parametric influences. The paper addresses this issue, presenting computationally efficient algorithms that extend the capabilities of simulation. The starting point is a model that captures the intricacies of hybrid systems, yet is suited to numerical integration. It will be shown that trajectory sensitivities are well defined for hybrid systems, and can be computed efficiently. These sensitivities allow the mapping of parameter uncertainty into approximate error bounds on nominal (piecewise smooth) trajectories. Furthermore, they provide gradient information that facilitates the solution of inverse problems. A range of problems will be considered, including shooting methods for locating (possibly non-smooth) limit cycles and grazing phenomena, and optimization algorithms for parameter estimation and controller tuning.

Keywords— Hybrid dynamical systems, inverse problems, parameter uncertainty, shooting methods, trajectory sensitivities.

1 Introduction

Tools for systematically exploring large disturbance behaviour of hybrid dynamical systems, such as power systems, are quite limited. Generally such analysis relies on time domain simulation and intuition. Whilst simulation provides a vast amount of information describing the behaviour of system states, it fails to provide insights into underlying parametric influences. Furthermore, it often fails to (directly) address the questions of importance to analysts.

Normal simulation-based investigations are limited to *forward problems*. The system model and parameters are given, and the corresponding system dynamic response is determined. However analysis frequently takes the form of *inverse problems* (Groetsch, 1999; Kirsch, 1996). In this case, the output is specified, and the problem is to determine parameters that induce (as closely as possible) the desired behaviour. System identification epitomizes this class of problems. Other forms of inverse problems abound though, with the paper considering, for example, the locating of limit cycles and *grazing* phenomena (Donde and Hiskens, 2006). In the context of hybrid systems, such problems are traditionally addressed by *ad hoc* repetition of forward (simulation) problems. The paper shows that systematic modelling establishes a foundation for algorithms that directly address inverse problems.

The paper is structured as follows. An overview of hybrid system modelling is provided in Section 2, and trajectory sensitivity concepts are presented in Section 3. Trajectory approximation and parameter uncertainty are discussed in Section 4, and various inverse problems are considered in Section 5. Conclusions are provided in Section 6.

2 Model

Systems that exhibit intrinsic interactions between continuous dynamics and discrete events have become known generically as *hybrid dynamical systems* (Liberzon, 2003; van der Schaft and Schumacher, 2000; Branicky et al., 1998). Numerous formal models, such as petri nets (David and Alla, 1992) and hybrid automata (van der Schaft and Schumacher, 2000), exist for rigorously describing hybrid system dynamics. However, those representations are not immediately amenable to numerical implementation. Analysis of large systems, such as power systems, requires a non-restrictive model formulation that is capable of capturing the full range of continuous/discrete hybrid system dynamics, yet is computationally efficient.

It was shown in (Hiskens, 2004; Hiskens and Pai, 2000) that these specifications can be met by a model that consists of a set of differential-algebraic equations, adapted to incorporate switching of the algebraic equations, and impulsive (state reset) action. This <u>DA</u> <u>Impulsive</u> <u>Switched</u> (DAIS) model has its genesis in the familiar DAE model

$$\dot{x} = f(x, y) \qquad (1)$$
$$0 = g(x, y) \qquad (2)$$

where $x \in \mathbb{R}^n$ are dynamic states, $y \in \mathbb{R}^m$ are algebraic states, $f : \mathbb{R}^{n+m} \to \mathbb{R}^n$, and $g : \mathbb{R}^{n+m} \to \mathbb{R}^m$.

Switching events can be incorporated into the DAE model by requiring the algebraic equations (2) to switch between sets of equations that describe pre- and post-event conditions. Considering a single switching event, (2) can be replaced

by

$$0 = g(x,y) \triangleq \begin{cases} g^-(x,y) & s(x,y) < 0 \\ g^+(x,y) & s(x,y) > 0, \end{cases} \quad (3)$$

where the superscripts '−' and '+' index the two sets of algebraic equations.[1] A switching event coincides with a zero crossing of the trigger function $s(x,y)$. Note that the concept of crossing is important. If the trajectory just touches (grazes) the triggering surface

$$\mathcal{S} = \{(x,y) : s(x,y) = 0\} \quad (4)$$

then behaviour beyond that point is indeterminant, as switching may or may not occur (Donde and Hiskens, 2005). Therefore the following assumption is required.

Assumption 1: The trajectory encounters the triggering surface $\mathcal{S}$ transversally.

The precise behaviour of the model at a switching event is not well defined by (3), and requires further explanation. Let the event occur at trigger time τ, and define τ^- as the time instant just prior to τ, and τ^+ as the instant just after τ. The limit values of the states can then be expressed as,

$$x^- \equiv x(\tau^-) := \lim_{t\uparrow\tau} x(t), \quad x^+ \equiv x(\tau^+) := \lim_{t\downarrow\tau} x(t) \quad (5)$$

$$y^- \equiv y(\tau^-) := \lim_{t\uparrow\tau} y(t), \quad y^+ \equiv y(\tau^+) := \lim_{t\downarrow\tau} y(t), \quad (6)$$

where $t \uparrow \tau$ implies $t < \tau$ approaches τ from below, and $t \downarrow \tau$ implies $t > \tau$ approaches τ from above. Clearly, two sets of variables (x^-, y^-) and (x^+, y^+) are required to fully describe behaviour at an event (Lee and Zheng, 2005).

By definition $s(x^-, y^-) = 0$, but $s(x^+, y^+)$ may not necessarily equal zero. Furthermore, assume without loss of generality that $s(x(t), y(t)) < 0$ for $t < \tau$. Then well defined switching behaviour requires $s(x(t), y(t)) > 0$ for $t > \tau$. Also, this sign assumption implies $g^-(x^-, y^-) = 0$ and $g^+(x^+, y^+) = 0$. Dynamic states are unaltered at a switching event, so $x^- = x^+$. In order to satisfy the altered algebraic equations, however, often $y^- \neq y^+$.

Switching events cannot efficiently capture all forms of discrete behaviour. Modelling approximations that introduce discrete jumps into the dynamic x-states are often convenient. Such behaviour has the form of an impulse, and can be described by a reset equation

$$x^+ = h(x^-, y^-) \quad \text{when } s(x,y) = 0, \quad (7)$$

[1]The functions g^- and g^+ may themselves have a switched form, resulting in a hierarchical switching structure.

where $h : \mathbb{R}^{n+m} \to \mathbb{R}^n$. The superscript notation is consistent with earlier use, with x^+ denoting the value of x just after the reset event, while x^- and y^- refer to the values of x and y just prior to the event. As in the case of a switching event, a reset event is triggered when $s(x,y)$ passes through zero. Away from that zero crossing condition, the evolution of the dynamic x-states is described by the differential equations (1).

Dynamic behaviour, generated numerically by simulation, can be described analytically by the *flow*,

$$x(t) = \phi(x_0, t) \quad (8)$$
$$y(t) = \psi(x_0, t). \quad (9)$$

Initial conditions imply

$$\phi(x_0, t_0) = x_0 \quad (10)$$
$$g(\phi(x_0, t_0), \psi(x_0, t_0)) = 0. \quad (11)$$

A compact development of trajectory sensitivities results from incorporating parameters $p \in \mathbb{R}^\ell$ into the dynamic states x. (Numerical implementation is also simplified.) This is achieved by introducing trivial differential equations

$$\dot{p} = 0 \quad (12)$$

into (1), and results in the natural partitioning

$$x = \begin{bmatrix} \underline{x} \\ p \end{bmatrix}, \qquad f = \begin{bmatrix} \underline{f} \\ 0 \end{bmatrix}, \qquad h = \begin{bmatrix} \underline{h} \\ p \end{bmatrix} \quad (13)$$

where $\underline{x}$ are the true dynamic states, and p are parameters. Accordingly, initial conditions and parameters will be treated synonymously throughout the remainder of the paper.

3 Trajectory Sensitivity

3.1 Motivation

The functional form of the flow (8)-(9) motivates the Taylor series expansions,

$$\phi(x_0 + \Delta x_0, t) = \phi(x_0, t) + \frac{\partial \phi(x_0, t)}{\partial x_0} \Delta x_0 + \mathcal{E}^\phi(x_0, t, \Delta x_0) \quad (14)$$

$$\psi(x_0 + \Delta x_0, t) = \psi(x_0, t) + \frac{\partial \psi(x_0, t)}{\partial x_0} \Delta x_0 + \mathcal{E}^\psi(x_0, t, \Delta x_0) \quad (15)$$

where $\mathcal{E}^\phi$ and $\mathcal{E}^\psi$ capture the higher order terms. For small $\|\Delta x_0\|$, the higher order terms may be neglected, giving

$$\Delta x(t) = \phi(x_0 + \Delta x_0, t) - \phi(x_0, t)$$
$$\approx \frac{\partial \phi(x_0, t)}{\partial x_0} \Delta x_0 \equiv \Phi(x_0, t) \Delta x_0 \quad (16)$$

$$\Delta y(t) = \psi(x_0 + \Delta x_0, t) - \psi(x_0, t)$$
$$\approx \frac{\partial \psi(x_0, t)}{\partial x_0} \Delta x_0 \equiv \Psi(x_0, t) \Delta x_0 \quad (17)$$

where Φ and Ψ are the *sensitivity transition matrices*, or *trajectory sensitivities*, associated with the x and y flows (Frank, 1978). Equation (16) describes the approximate change $\Delta x(t)$ in a trajectory, at time t along the trajectory, for a given small change in initial conditions $\Delta x_0^\top = [\Delta \underline{x}_0^\top \ \Delta p^\top]$. Likewise, the change $\Delta y(t)$ is given by (17).

3.2 Variational equations

Away from events, where system dynamics evolve smoothly, the sensitivities Φ and Ψ are obtained by differentiating (1)-(2) with respect to x_0. This gives

$$\dot{\Phi} = f_x(t)\Phi + f_y(t)\Psi \qquad (18)$$
$$0 = g_x(t)\Phi + g_y(t)\Psi \qquad (19)$$

where $f_x \equiv \partial f / \partial x$, and likewise for the other Jacobian matrices. Note that f_x, f_y, g_x, g_y are evaluated along the trajectory, and hence are time-varying matrices. The computational burden of numerically integrating this (potentially high order) linear time-varying DAE system is minimal though. It is shown in (Feehery et al., 1997; Hiskens and Pai, 2000; Li et al., 2000) that when an implicit numerical integration technique such as trapezoidal integration is used, the solution of (18)-(19) can be obtained as a by-product of computing the underlying trajectory.

Initial conditions for Φ are obtained from (10) as

$$\Phi(x_0, t_0) = I \qquad (20)$$

where I is the identity matrix. Initial conditions for Ψ follow directly from (19),

$$0 = g_x(t_0) + g_y(t_0)\Psi(x_0, t_0). \qquad (21)$$

Equations (18)-(19) describe the evolution of the sensitivities Φ and Ψ between events. However the sensitivities are often discontinuous at events. It is necessary to calculate *jump conditions* describing event-induced step changes in Φ and Ψ. Consider the most general case of a coincident switching/reset event, described by (3) and (7). (The jump conditions appropriate for separate switching or reset events follow directly from this more general situation.) It was shown by Hiskens and Pai (2000) that the jump conditions for the sensitivities Φ are given by

$$\Phi(x_0, \tau^+) = h_x^* \Phi(x_0, \tau^-) - \left(f^+ - h_x^* f^-\right) \tau_{x_0} \qquad (22)$$

where

$$\tau_{x_0} \equiv \frac{\partial \tau}{\partial x_0} = -\frac{s_x^* \Phi(x_0, \tau^-)}{s_x^* f^-} \qquad (23)$$

and

$$f^- \equiv f(x^-, y^-) \qquad (24)$$
$$f^+ \equiv f(x^+, y^+) \qquad (25)$$
$$h_x^* = \left.\left(h_x - h_y g_y^{-1} g_x\right)\right|_{\tau^-} \qquad (26)$$
$$s_x^* = \left.\left(s_x - s_y g_y^{-1} g_x\right)\right|_{\tau^-}. \qquad (27)$$

Note that jump conditions are only well defined when Assumption 1 is satisfied. Otherwise, if the trajectory encounters $\mathcal{S}$ tangentially rather than transversally, the denominator of (23) will equal zero. The sensitivities Ψ immediately after the event are given by

$$\Psi(x_0, \tau^+) = -\left.\left(g_y^{-1} g_x\right)\right|_{\tau^+} \Phi(x_0, \tau^+). \qquad (28)$$

Keep in mind that g in (26)-(27) refers to its pre-event form, whereas post-event conditions apply in (28).

Subsequent to the event, for $t > \tau^+$, calculation of the sensitivities proceeds according to (18)-(19). The jump conditions (22) and (28) provide the initial conditions for this post-event integration.

4 Parameter Uncertainty

4.1 Trajectory approximation

For general nonlinear systems, the flow functions ϕ and ψ, given by (8)-(9), cannot be expressed in closed form. Any change in initial conditions (and/or parameters) therefore requires a complete re-simulation of the dynamic model. However if changes are relatively small, the computational effort of repeated simulation can be avoided by forming approximate trajectories.

Rearranging (16)-(17) gives the first-order approximations of the flow,

$$\phi(x_0 + \Delta x_0, t) \approx \phi(x_0, t) + \Phi(x_0, t)\Delta x_0 \qquad (29)$$
$$\psi(x_0 + \Delta x_0, t) \approx \psi(x_0, t) + \Psi(x_0, t)\Delta x_0. \qquad (30)$$

As mentioned previously, the trajectory sensitivities Φ and Ψ can be computed efficiently as a byproduct of simulating the nominal trajectory. Therefore a range of (approximate) perturbed trajectories are available via (29)-(30) for the computational cost of a single nominal trajectory. This computational efficiency will be exploited in Section 4.2 to explore the influence of parameter uncertainty.

The single machine infinite bus system of Figure 1 will be used to illustrate the quality of trajectory approximation achievable by (29)-(30). The generator in this system was represented by a sixth order machine model (Sauer and Pai, 1998). Its AVR/PSS was modelled according to the IEEE standard representation shown in Figure 2. The system was subjected to a balanced three phase
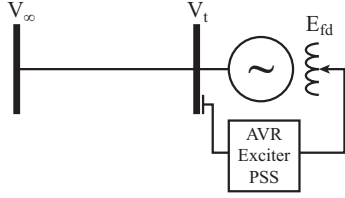
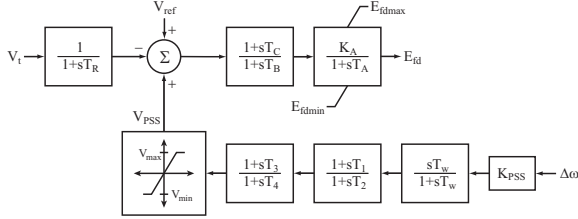Figure 1: Single machine infinite bus system.

Figure 2: AVR/PSS standard models.

Figure 3: Field voltage behaviour: comparison of actual and approximate trajectories.

fault on the generator terminal bus. The fault was cleared without line tripping.

The nominal trajectory, shown in Figure 3 as a dashed line, was obtained for a fault clearing time of $t_{cl} = 0.23$ sec, and a maximum field voltage limit of $E_{fd,max} = 5.8$ pu. Notice that behaviour is quite non-smooth, due to the fault and limit-related events.

Trajectory sensitivities were used to synthesize the approximate behaviour that would occur for altered parameter values $t_{cl} = 0.21$ sec and $E_{fd,max} = 5.0$ pu (cf. the original values of 0.23 sec and 5.8 pu respectively.) This synthesized trajectory is shown as the solid line in Figure 3. For comparison purposes, the full simulation was repeated using these altered parameters. The corresponding trajectory is shown as a dash-dot line in Figure 3.

The parameters chosen for this illustration exert a significant nonlinear, non-smooth influence on system behaviour. However, even though the change in these parameters is large, the approximated trajectory closely tracks the actual perturbed trajectory.

4.2 Bounding parallelotopes

It is common for models of real-world systems to involve parameters that are not known with certainty. In the case of power systems, for example, load behaviour is notoriously difficult to model accurately. A thorough understanding of the influence of uncertain parameters requires many simulations. However the computational effort involved in each simulation generally precludes anything more than a cursory examination of parametric dependencies.

Trajectory approximations, given by (29)-(30), overcome the need for repetitive simulation, though at the cost of some loss 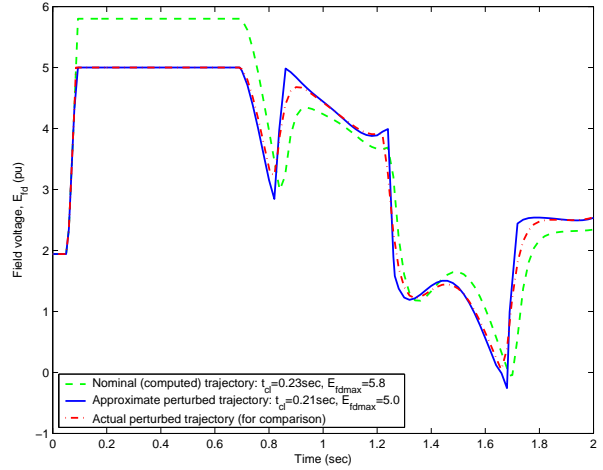of accuracy. The affine nature of (29)-(30) allows straight-forward approaches to quantifying the effects of uncertainty. Worst-case analysis is considered here, with probabilistic assessment discussed in (Hiskens and Alseddiqui, 2006).

Under a worst-case scenario, uncertain parameters may lie anywhere within the (convex) orthotope[2]

$$\mathcal{B} = \{\Delta x_0 : \Delta_{min} \leq \Delta x_0 \leq \Delta_{max}\} \qquad (31)$$

where Δx_0 describes the deviations from the nominal parameter values, Δ_{min} and Δ_{max} are vectors of minimum and maximum allowable deviations respectively, and the inequalities are on an element by element basis. The dimension of the orthotope $\mathcal{B}$ matches the number of uncertain parameters. Its vertices are extremes where every element of Δx_0 takes either its maximum or minimum value. Trajectory approximations (29)-(30) describe a time-dependent affine transformation of initial conditions $\Delta x_0 \in \mathcal{B}$, provided the following assumption is satisfied.

Assumption 2: All trajectories emanating from the set $x_0 + \mathcal{B}$ have the same event *history*, i.e., the same events occur and in the same order.

Under the affine transformations (29)-(30), the orthotope $\mathcal{B}$ is shifted and distorted to form time-dependent parallelotopes[3]

$$\mathcal{P}^\phi(t) = \phi(x_0, t) + \Phi(x_0, t)\mathcal{B} \qquad (32)$$

$$\mathcal{P}^\psi(t) = \psi(x_0, t) + \Psi(x_0, t)\mathcal{B}. \qquad (33)$$

Importantly, the affine transformation maintains convexity (Rockfellar, 1970), with vertices of $\mathcal{B}$

---

[2]An orthotope is a high dimensional generalization of a rectangle (Coxeter, 1973).

[3]A parallelotope is a high dimensional generalization of a parallelogram (Coxeter, 1973). Parallel faces remain parallel under the affine transformation, but orthogonality of adjacent faces is lost. Full details can be found in (Brøndsted, 1983).
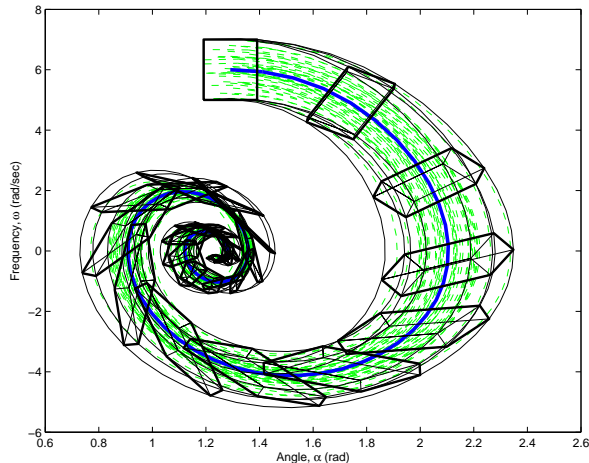
Figure 4: Phase portrait view of parallelotope propagation.

Figure 5: Parameter estimation.

mapping to vertices of $\mathcal{P}^{\phi}(t)$ and $\mathcal{P}^{\psi}(t)$. Therefore, (32)-(33) describe the propagation of a convex set through state space. Initial conditions that lie within $x_0 + \mathcal{B}$ give rise to (approximate) trajectories that remain within the time-propagated parallelotopes.

To illustrate, the power system example of Figure 1 will be used, though with the AVR/PSS limits (see Figure 2) disabled. The thicker solid trajectory in Figure 4 shows the angle-frequency phase portrait when all states are initially in steady-state, except for $\omega(t_0) = 6$ rad/sec. An error bound of $-0.1 \leq \Delta\alpha(t_0) \leq 0.1$ was chosen for the initial value of the angle α, and $-1 \leq \Delta\omega(t_0) \leq 1$ for frequency ω. Also, it was assumed the generator inertia could be in error by $-0.075 \leq \frac{\Delta H}{H} \leq 0.075$. This initial error orthotope $\mathcal{B}$ is projected onto the $\alpha - \omega$ plane as the rectangle symmetrically surrounding the initial point of the nominal trajectory.

Figure 4 shows the propagation of $\mathcal{B}$ according to (32)-(33). The approximate trajectories emanating from the vertices of $\mathcal{B}$ are shown as thinner solid lines, while the distortion of $\mathcal{B}$ along the trajectory is shown as the sequence of parallelotopes. The projection onto the $\alpha - \omega$ plane flattens these parallelotopes. Their outline, or convex hull (Rockfellar, 1970), is shown as a darker line.

Forty sets of initial conditions were randomly selected from $x_0 + \mathcal{B}$, assuming a uniform distribution. The true (simulated) trajectories arising from those initial conditions are shown as lighter dashed lines. It can be seen that these trajectories lie (almost completely) within the region covered by the propagated parallelotopes, the outline of which is given by the approximate trajectories arising from the vertices of $\mathcal{B}$.
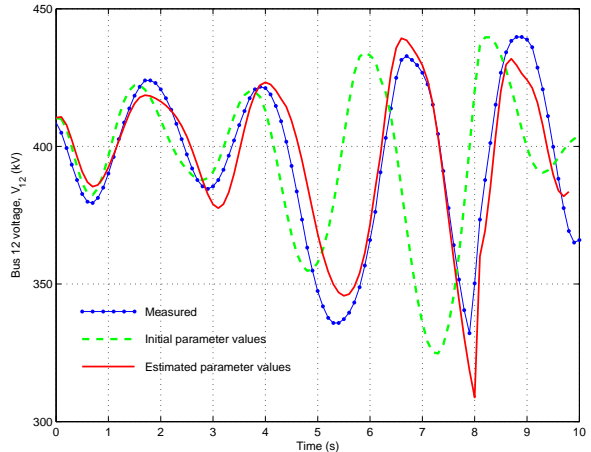
5 Applications

5.1 Parameter estimation

Parameter estimation is a huge field. Even so, for hybrid systems that do not possess special structure, such as power systems, parameter estimation typically reverts to iterative solution of Gauss-Newton based algorithms. Such ideas are not new (Frank, 1978). The number of parameters that could be estimated using those earlier ideas was limited though, because trajectory sensitivities were generated numerically. By exploiting more computationally efficient methods of calculation (Hiskens and Pai, 2000), it is possible to consider many system-wide parameters. Furthermore, the extension of trajectory sensitivities to hybrid systems allows parameters associated with discontinuities to be estimated. Figure 5 provides an illustration.

A voltage measurement from an actual disturbance on the Nordel system (Hiskens and Akke, 1999; Hiskens, 2001) is shown. The figure also shows the simulated voltage trajectory obtained using the utility's "standard" parameter values. This set of parameters did not predict behaviour particularly well. The single voltage measurement was therefore used to estimate a number of parameters, including the switching time of an important reactor. Figure 5 shows that this resulted in a much closer match between simulated and measured response.

5.2 Dynamic embedded optimization

Optimization problems arise frequently in the analysis of dynamical systems. In power systems, for instance, examples range from tuning generator AVR/PSSs to determining the optimal location, amount and switching times for load shedding (Moors and Van Cutsem, 1999). Most problems can be formulated using a Bolza form of ob-

jective function

$$\min_{\theta, t_f} \mathcal{J}(x, y, \theta, t_f) \qquad (34)$$

where

$$\mathcal{J} = \mathcal{K}\big(x(t_f), y(t_f), \theta, t_f\big) + \int_{t_0}^{t_f} \mathcal{L}\big(x(t), y(t), \theta, t\big) dt, \qquad (35)$$

θ are the design parameters, i.e., the parameters adjusted to achieve the objective, and t_f is the final time.

The solution of (34) for hybrid systems is complicated by discontinuous behaviour at events. However those complications largely disappear under the assumption that the order of events does not change as θ and t_f vary. This assumption is common throughout the literature, though it is expressed in various ways: transversal crossings of triggering hypersurfaces were assumed by Branicky et al. (1998), existence of trajectory sensitivities was assumed by Galán and Barton (1998), and Piccoli (1998) assumed all flows have the same *history*. All statements are equivalent.

Under that assumption, and other mild assumptions, it was concluded by Piccoli (1998) that if $\mathcal{J}$ is continuous in its arguments then a solution to (34) exists. Furthermore, Galán and Barton (1998) showed that if $\mathcal{J}$ is a smooth function of its arguments, then it is continuously differentiable with respect to θ and t_f. The minimization can therefore be solved using gradient-based methods. Trajectory sensitivities, as provided by the DAIS model, underlie the gradient information.

If the event ordering assumption is not satisfied, $\mathcal{J}$ may be discontinuous. The optimization problem then takes on a combinatorial nature, as each continuous section of $\mathcal{J}$ must be searched for a local minimum.

Non-traditional design capabilities arise from embedding the DAIS model within the optimization framework (34)-(35). To illustrate, consider the generator AVR/PSS shown in Figure 2. Typically PSS output limits are assigned on an *ad hoc* basis. However Hiskens (2002) determined optimal limit values by establishing a cost function (35) that maximized damping whilst minimizing deviations in the generator terminal voltage. Figure 6 compares optimal performance with that obtained using standard limit values. (Note that only the limit values differ between these two cases. All other parameters are fixed.)

5.3 Shooting methods

System analysis is often tantamount to understanding the influence of parameters on system behaviour, and applying that knowledge to achieve a desired outcome. The "known" information is the desired outcome. The parameters that achieve
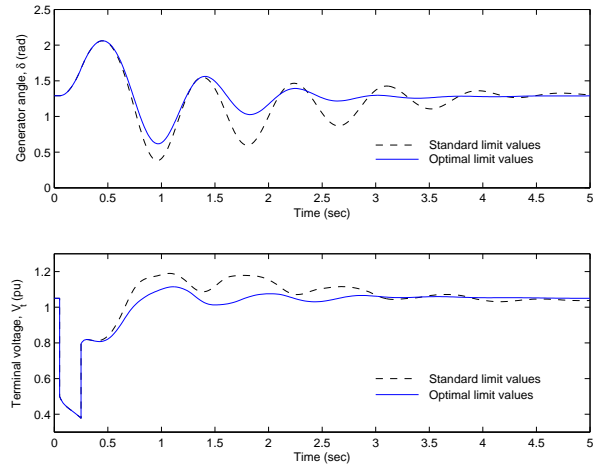

Figure 6: Generator angle response.

that outcome must be deduced. Such inverse problems can often be formulated as

$$F(z) = 0 \qquad (36)$$

where F incorporates the flows ϕ and ψ. Two important cases are considered below, namely locating limit cycles, and determining conditions that induce grazing, though other applications abound.

Nonlinear problems of the form (36) can be solved using Newton's method, though in this case evaluation of F involves numerical integration. For that reason, solution processes are known as shooting methods (Seydel, 1994; Stoer and Bulirsch, 1993). The Jacobian DF required by Newton's method incorporates trajectory sensitivities Φ and Ψ, which must be evaluated in conjunction with the numerical integration.

5.4 Limit cycles

Periodic (limit cycle) behaviour occurs in a wide variety of systems, from biological processes to power systems. Limit cycles and their stability are determined using Poincaré maps (Seydel, 1994; Parker and Chua, 1989). A Poincaré map effectively samples the flow of a periodic system once every period. The concept is illustrated in Figure 7.

To define a Poincaré map, consider the limit cycle Γ shown in Figure 7. Let Σ be a hyperplane transversal to Γ and defined by

$$\Sigma = \{x : \sigma^\top (x - \tilde{x}) = 0\} \qquad (37)$$

where $\tilde{x}$ is a point anchoring Σ, and σ is a vector normal to Σ. The trajectory emanating from x^* will again encounter Σ at x^* after T seconds, where T is the minimum period of the limit cycle. The existence of trajectory sensitivities ensures continuity of the flow ϕ with respect to initial conditions. Therefore trajectories starting on Σ in a neighbourhood of x^* will, in approximately
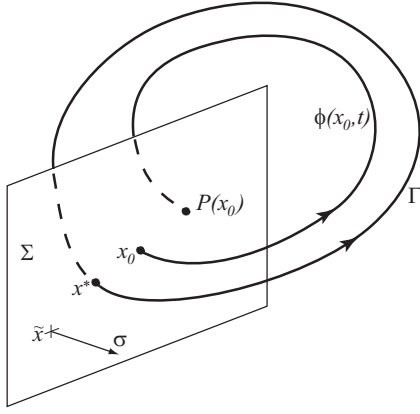
Figure 7: Poincaré map.

Figure 8: Trajectory grazing triggering hypersurface.

T seconds, intersect Σ in the vicinity of x^*. Hence ϕ and Σ define the Poincaré map

$$x_{k+1} = P(x_k) := \phi(x_k, \tau_r(x_k)) \qquad (38)$$

where $\tau_r(x_k) \approx T$ is the time taken for the trajectory to return to Σ. Complete details can be found in (Seydel, 1994; Parker and Chua, 1989). Note that the Poincaré map is well defined even though the underlying flow may be non-smooth.

From (38), it can be seen that a point x^* on the limit cycle can be located using Newton's method to solve the nonlinear algebraic equations

$$F_l(x^*) = \phi(x^*, \tau_r(x^*)) - x^* = 0. \qquad (39)$$

5.5 Grazing

Grazing refers to situations where the trajectory just touches a triggering hypersurface. Figure 8 provides an illustration. At a parameter value θ_g, lying between θ_{hit} and θ_{miss}, the trajectory tangentially encounters (*grazes*) the triggering hypersurface. This bounding case separates trajectories that encounter the hypersurface from those that do not.

A grazing trajectory must touch the target hypersurface, which can be described by[4]

$$b(x) = 0. \qquad (40)$$

Furthermore, the trajectory must be tangential to the hypersurface at the point of contact. It follows from (1) and (40) that tangential contact is described by

$$\nabla b(x_g)^\top f(x_g, y_g) = 0, \qquad (41)$$

as $f(x_g, y_g)$ specifies the trajectory direction at the grazing point. Collecting together appropriate

equations, a grazing point is described by

$$\phi(x_0(\theta), t_g) - x_g = 0 \qquad (42)$$
$$b(x_g) = 0 \qquad (43)$$
$$\nabla b(x_g)^\top f(x_g, y_g) = 0 \qquad (44)$$
$$g(x_g, y_g) = 0. \qquad (45)$$

This set of equations can be solved using a shooting method. Full details are provided in (Donde and Hiskens, 2006), with a similar development given by Zhao et al. (2004).

5.6 Example

The single machine infinite bus system of Figure 1 was used to explore the existence and nature of limit cycles. It was found that a Hopf bifurcation occurs at an AVR gain of $K_A^* = 208.22$. The equilibrium point is unstable for $K_A > 208.22$. For example, with a gain of $K_A = 212$, linearization around the equilibrium point gave an unstable eigenvalue pair of $0.0053 \pm j5.86$. However it was found that the unstable behaviour was restricted by the field voltage limit $E_{fdmax} = 5.4$, with behaviour stabilizing to a non-smooth limit cycle.

The shooting method of Section 5.4 was used to locate this stable limit cycle. It was found that all characteristic multipliers lay within the unit circle, with the largest having a magnitude of 0.83. This confirmed the limit cycle was indeed an attractor.

Further investigation of the Hopf bifurcation revealed that it was in fact supercritical. The bifurcation diagram of Figure 9, produced using the continuation process of (Donde and Hiskens, 2006), shows a branch of stable limit cycles emanating from the Hopf bifurcation.[5] This branch of limit cycles undergoes a cyclic fold at $K_A = 209.9$, beyond which the branch comprises unstable limit cycles.

---

[4]The more general case of $b(x, y) = 0$ is presented in (Donde and Hiskens, 2006). The dependence on algebraic variables y is neglected here to simplify the presentation.
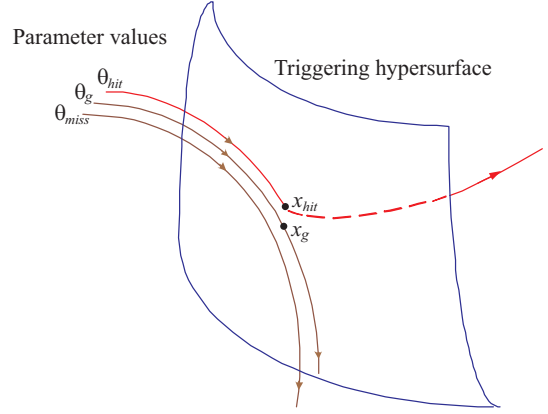
[5]The limit cycles are presented in Figure 9 as dots that give the extreme values of E_{fd}.

Figure 9: Bifurcation diagram.
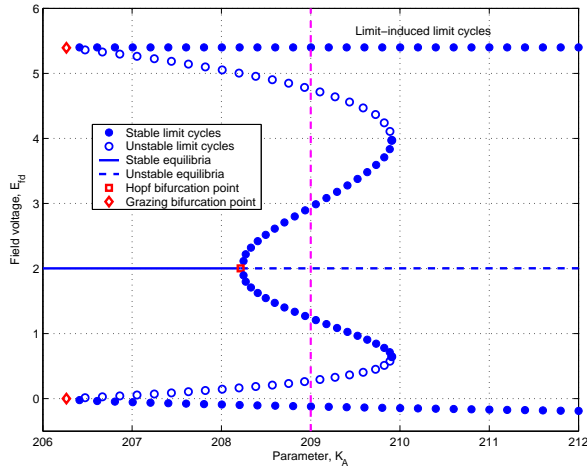

Figure 10: Co-existing limit cycles and equilibrium point, $K_A = 209$.

As shown in Figure 9, the stable non-smooth limit cycles, induced by the E_{fdmax} limit, coexist with the smooth limit cycles that result from the Hopf bifurcation. Over the range $208.22 < K_A < 209.9$, the system exhibits an unstable equilibrium point, an unstable limit cycle, and two stable limit cycles (one smooth and one non-smooth). These limit sets are shown in Figure 10, for a gain $K_A = 209$.

The shooting method of Section 5.4 was used to obtain the limit cycles of Figure 10. In all cases, convergence was obtained in three iterations, with each iteration requiring a single simulation of one period of the oscillation. On the other hand, reliance on time-domain simulation would be futile. The unstable limit cycle has characteristic multipliers both inside and outside the unit circle, so time reversal would not achieve convergent behaviour. Furthermore, transient behaviour is poorly damped in the vicinity of the Hopf bifurcation. Therefore lengthy simulation would be required for adequate convergence to the stable limit cycles. Shooting methods are however unaffected by the stability properties and damping associated with a limit cycle.

As the gain K_A was reduced, the branches of limit-induced and smooth limit cycles converged to a point where the smooth limit cycle became tangential to (grazed) the E_{fdmax} surface. Using the shooting method of (Donde and Hiskens, 2006), it was found that this grazing limit cycle occurred at $K_A = 206.26$. As K_A reduced towards this critical value, the non-smooth limit cycle spent less and less time on the E_{fdmax} surface. Correspondingly, one of its characteristic multipliers approached unity. The smooth and non-smooth limit cycles coalesced at grazing. As K_A was further reduced beyond the grazing value, the limit cycles vanished, with structural stability lost due to a grazing bifurcation (di Bernardo et al., 2001).
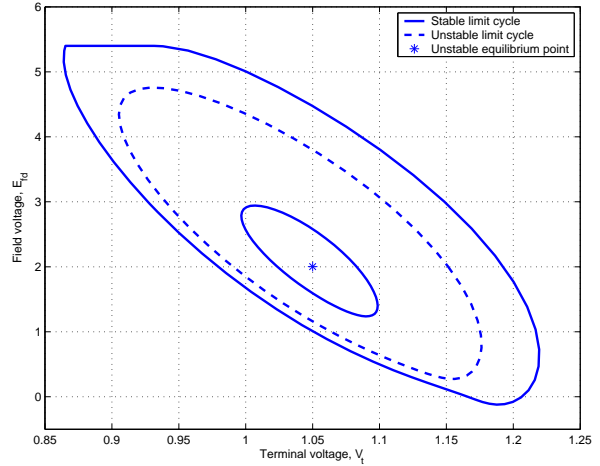
6 Conclusions

The dynamic response of many real-world systems involves interactions between continuous dynamics and discrete events. Such hybrid behaviour can be captured by a model that consists of a set of differential-algebraic equations, modified to incorporate impulse (state reset) action and constraint switching (DAIS model).

For such systems, analysis of large disturbance behaviour is largely reliant on time domain simulation. Underlying parametric influences cannot, however, be easily deduced from such analysis. The paper proposes the use of trajectory sensitivities to complement time domain analysis. Trajectory sensitivities can be obtained as a by-product of implicit numerical integration techniques, incurring little additional computational cost.

Trajectory sensitivities facilitate trajectory approximations that enable efficient assessment of parameter uncertainty. Furthermore, trajectory sensitivities provide gradient information that underlies a number of inverse problems, including parameter estimation, dynamic embedded optimization, and shooting methods.

References

Branicky, M., Borkar, V. and Mitter, S. (1998). A unified framework for hybrid control: Model and optimal control theory, *IEEE Transactions on Automatic Control* **43**(1): 31–45.

Brøndsted, A. (1983). *An Introduction to Convex Polytopes*, Springer-Verlag, New York.

Coxeter, H. (1973). *Regular Polytopes*, 3rd edn, Dover, New York.

David, R. and Alla, H. (1992). *Petri Nets and Grafecet*, Prentice-Hall, Englewood Cliffs, NJ.

di Bernardo, M., Budd, C. and Champneys, A. (2001). Grazing and border-collision in piecewise-smooth systems: A unified analytical framework, *Physical Review Letters* **86**(12): 2553–2556.

Donde, V. and Hiskens, I. (2005). Dynamic performance assessment: Grazing and related phenomena, *IEEE Transactions on Power Systems* **20**(4): 1967–1975.

Donde, V. and Hiskens, I. (2006). Shooting methods for locating grazing phenomena in hybrid systems, *International Journal of Bifurcation and Chaos* **16**(3): 671–692.

Feehery, W., Tolsma, J. and Barton, P. (1997). Efficient sensitivity analysis of large-scale differential-algebraic systems, *Applied Numerical Mathematics* **25**: 41–54.

Frank, P. (1978). *Introduction to System Sensitivity Theory*, Academic Press, New York.

Galán, S. and Barton, P. (1998). Dynamic optimization of hybrid systems, *Computers chem. Engng* **22, Suppl.**: S183–S190.

Groetsch, C. (1999). *Inverse problems: activities for undergraduates*, Mathematical Association of America.

Hiskens, I. (2001). Nonlinear dynamic model evaluation from disturbance measurements, *IEEE Transactions on Power Systems* **16**(4): 702–710.

Hiskens, I. (2002). Systematic tuning of nonlinear power system controllers, *Proceedings of the 2002 IEEE International Conference on Control Applications*, Glasgow, Scotland, pp. 19–24.

Hiskens, I. (2004). Power system modeling for inverse problems, *IEEE Transactions on Circuits and Systems I: Regular Papers* **51**(3): 539–551.

Hiskens, I. and Akke, M. (1999). Analysis of the Nordel power grid disturbance of January 1, 1997 using trajectory sensitivities, *IEEE Transactions on Power Systems* **14**(3): 987–994.

Hiskens, I. and Alseddiqui, J. (2006). Sensitivity, approximation and uncertainty in power system dynamic simulation, *IEEE Transactions on Power Systems* **21**(4).

Hiskens, I. and Pai, M. (2000). Trajectory sensitivity analysis of hybrid systems, *IEEE Transactions on Circuits and Systems I: Fundamental Theory and Applications* **47**(2): 204–220.

Kirsch, A. (1996). *An introduction to the mathematical theory of inverse problems*, Springer, Berlin.

Lee, E. and Zheng, H. (2005). Operational semantics of hybrid systems, *Hybrid Systems: Computation and Control*, M. Morari and L. Thiele (Editors), Lecture Notes in Computer Science, Vol. 3414, Springer, pp. 25–53.

Li, S., Petzold, L. and Zhu, W. (2000). Sensitivity analysis of differential-algebraic equations: A comparison of methods on a special problem, *Applied Numerical Mathematics* **32**(8): 161–174.

Liberzon, D. (2003). *Switching in Systems and Control*, Birkhauser, Boston.

Moors, C. and Van Cutsem, T. (1999). Determination of optimal load shedding against voltage instability, *Proceedings of the 13th Power Systems Computation Conference*, Vol. 2, Trondheim, Norway, pp. 993–1000.

Parker, T. and Chua, L. (1989). *Practical Numerical Algorithms for Chaotic Systems*, Springer-Verlag, New York, NY.

Piccoli, B. (1998). Hybrid systems and optimal control, *Proceedings of the 37th IEEE Conference on Decision and Control*, Tampa, FL.

Rockfellar, R. (1970). *Convex Analysis*, Princeton University Press, Princeton, NJ.

Sauer, P. and Pai, M. (1998). *Power System Dynamics and Stability*, Prentice Hall, Upper Saddle River, NJ.

Seydel, R. (1994). *Practical Bifurcation and Stability Analysis*, 2nd edn, Springer-Verlag, New York.

Stoer, J. and Bulirsch, R. (1993). *Introduction to Numerical Analysis*, 2nd edn, Springer, New York.

van der Schaft, A. and Schumacher, H. (2000). *An Introduction to Hybrid Dynamical Systems*, Springer-Verlag, London.

Zhao, X., Dankowicz, H., Reddy, C. and Nayfeh, A. (2004). Modeling and simulation methodology for impact microactuators, *Journal of Micromechanics and Microengineering* **14**: 775–784.